Journal of Marine Science and Technology

Volume 28 | Issue 2 Article 4

P-Y CURVE OF SMALL-SPACED ROW PILES SUBJECTED TO LATERAL LOADS IN MARINE CLAY

Runze Xue
National Engineering Laboratory for Port Hydraulic Construction Technology, Ministry of Transport. No.2618, No.2 Xingang Rd., Binhai New District, Tianjin, China. State Key Laboratory of Hydraulic Engineering Simulation and Safety, Tianjin University. No.92, Weijin Road, Nankai District, Tianjin, China.

Shean Bie
State Key Laboratory of Hydraulic Engineering Simulation and Safety, Tianjin University. No.92, Weijin Road, Nankai District, Tianjin, China., bieshean@tju.edu.cn

Linlin Guo
State Key Laboratory of Hydraulic Engineering Simulation and Safety, Tianjin University. No.92, Weijin Road, Nankai District, Tianjin, China.

Recommended Citation

Xue, Runze; Bie, Shean; and Guo, Linlin (2020) "P-Y CURVE OF SMALL-SPACED ROW PILES SUBJECTED TO LATERAL LOADS IN MARINE CLAY," *Journal of Marine Science and Technology*: Vol. 28: Iss. 2, Article 4.
DOI: 10.6119/JMST.202004_28(2).0004
Available at: https://jmstt.ntou.edu.tw/journal/vol28/iss2/4

P-Y CURVE OF SMALL-SPACED ROW PILES SUBJECTED TO LATERAL LOADS IN MARINE CLAY

Acknowledgements

This research was funded by the Tianjin Key R & D Plan (18YFZCSF00490) and the Tianjin marine development with science and technology project (Nos.KJXH2014-11). This research was supported by Tianjin Port Engineering Co. Ltd., which was responsible for engineering application construction. This manuscript was edited by Wallace Academic Editing.

Journal of Marine Science and Technology, Vol. 28, No. 2, pp. 105-119 (2020)
DOI: 10.6119/JMST.202004_28(2).0004

P-Y CURVE OF SMALL-SPACED ROW PILES SUBJECTED TO LATERAL LOADS IN MARINE CLAY

Runze Xue[1,2], Shean Bie[2] and Linlin Guo[2]

Key words: row piles; lateral load; small pile spacing; finite element analysis.

ABSTRACT

Newly proposed pile wall frame structures (PWFSs), notably with small-spaced row piles, have great potential for cofferdams of artificial islands applied for oil recovery in shallow seas. Studies have been called to analyze the bearing performance of small-spaced row piles subjected to lateral loads. A numerical investigation of laterally loaded row piles with small pile spacing was conducted to achieve a fitted algebraic expression of the *P-Y* curve. Significantly different from the hyperbolic *P-Y* curves of a single pile reported in other studies, the *P-Y* curve of small-spaced row piles is similar to an elastic–perfectly plastic curve, which simply depends on the ultimate lateral bearing capacity of piles (P_u) and initial slope of curves (K_i). Parametric studies have revealed that P_u and K_i values are affected by pile spacing, depth, untrained shear strength of soil, and relative soil–pile rigidity. Algebraic expression of the *P-Y* curve could be employed for the subgrade reaction method and be effectively used in predicting the behavior of small-spaced row piles, such as PWFSs.

I. INTRODUCTION

Pile wall frame structures (PWFSs; Li et al., 2013; Xue et al., 2019) are double-wall pile structures used in marine soft soil, with an integrally precast reinforced concrete framework adopted to connect double rows of piles into a whole, according to the PWFS schematic in Fig. 1. The PWFS pile base consists of two rows of prestressed high-strength concrete (PHC) pipe piles closely placed at intervals of 0.1–0.5 *d*. Prefabricated onshore and in-situ casted, PWFSs have the advantages of convenient construction, low project cost, and good structural integrity. PWFSs were employed for a workboat wharf and cofferdam in Tianjin Port and Binzhou Port, China, respectively. Moreover, PWFSs own potential to be applied as the permeable breakwater and cofferdams of artificial islands in shallow waters. As PWFSs are backfilled, the dominant load of structures is the lateral earth pressure aroused by elevation differences in soil surface, which merit investigation for small pile spacing effects on the lateral bearing capacity of row pile structures. Compared with double-row piles used for pit supporting, PWFSs have a larger row spacing of 9–12 *d*, which indicates pile spacing between front-row and rear-row piles. Because PWFS is laterally loaded, front-row piles bear considerably more load than do rear-row piles (Xue et al., 2019). Because row spacing is large, rear-row piles have little effect on front-row piles, causing similar *P-Y* curves between the two pile types. Therefore study mainly focused on the *P-Y* curve of single-row piles.

Studies on laterally loaded piles have mostly focused on single pile structures (Kim and Jeong, 2011; Rani and Prashant, 2015; Zhang et al., 2016; Zhang, 2018) or pile groups with pile spacing larger than 3 *d* (Chandrasekaran et al., 2010; Aminfar et al., 2015), and few have focused on the lateral bearing capacity of row pile structures with small pile spacing ($\delta/d < 3$), such as PWFSs. The lateral bearing capacity of pile groups is generally obtained by correcting the lateral bearing capacity of single piles with the group reduction factor. For pile groups with a pile spacing of 3 *d*, a group reduction factor of 0.3–0.7 for cohesionless soil based on numerical simulation was proposed by Fayyazi et al. (2014), and 0.25–0.6 for elastic soil was determined by Salgado et al. (2014) through theoretical deduction.

The stress–strain relationship curve of soils obtained from triaxial tests reveals that strain increments caused by equal stress increments are not commensurate at different stress levels. McClelland and Focht (1958) first developed a load–displacement curve known as the *P-Y* curve to describe the nonlinear behavior of laterally loaded piles in undisturbed clay. A hyperbolic *P-Y* curve for cohesive soil was established through laboratory triaxial tests conducted by Konder (1963).

Paper submitted 04/30/19; revised 10/30/19; accepted 02/24/20. Corresponding Author: Shean Bie (Email: bieshean@tju.edu.cn)
[1] National Engineering Laboratory for Port Hydraulic Construction Technology, Ministry of Transport. No.2618, No.2 Xingang Rd., Binhai New District, Tianjin, China
[2] State Key Laboratory of Hydraulic Engineering Simulation and Safety, Tianjin University. No.92, Weijin Road, Nankai District, Tianjin, China.

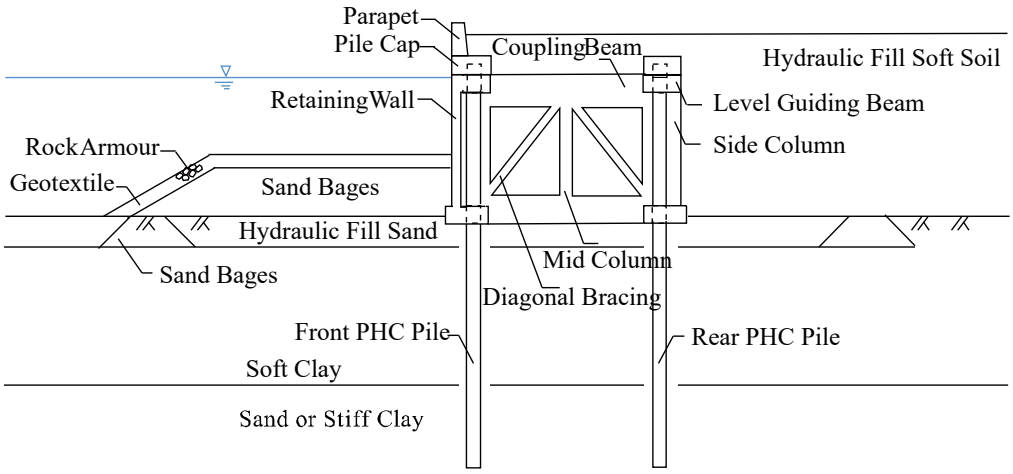

(a) Cross-sectional view

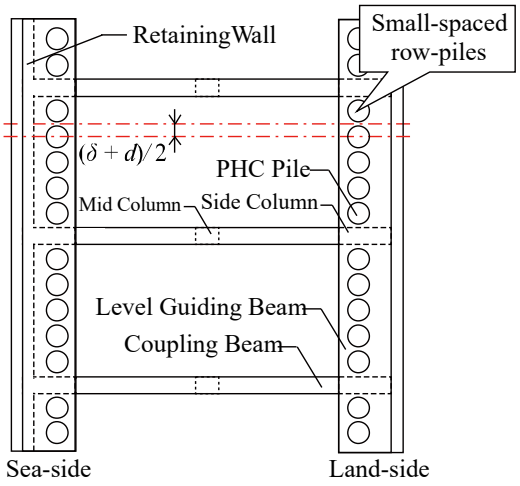

(b) Plan view of PWFSs

Fig. 1. Schematic of PWFSs as a cofferdam.

From a physical model test and theoretical analysis, *P-Y* curve expressions for laterally loaded piles in soft and stiff soil were proposed by Matlock (1970) and Reese et al. (1975). Uniform expression of the *P-Y* curve in clay was achieved through comprehensive analysis conducted by Sullivan et al. (1980). Forms of the *P-Y* curve function were presented to improve the prediction accuracy of pile behaviors regarding various soil conditions, load types, and pile spacing (Wang and Wu, 1991; Wu et al. 1998; Jeong et al. 2011; Zhu et al. 2015; Su et al. 2017).

The progression of computer technology strongly promotes research on pile–soil interaction by using rigorous finite element analysis (FEA). Three-dimensional (3D) soil continuity can be considered in FEA to quantitatively investigate effects on laterally loaded pile on factors such as the elastoplastic constitutive relationship among soil, pile–soil contact surface properties, boundary conditions, and construction steps (Conte et al., 2013; Khodair and Abdel-Mohti, 2014). The feasibility of a finite element method based on the Mohr–Coulomb soil constitutive model with the nonassociated flow rule has been proven (Peng et al., 2010; Kim and Jeong, 2011; Murphy et al., 2018).

The *P-Y* curve of laterally loaded row piles was numerically investigated in this study, particularly for those with small pile spacing ($\delta/d < 3$). A series of 3D finite element models of single-row piles subjected to lateral loads in marine clay was established, with pile spacing varying from 8–0.1 d for pile–soil interaction continuity and pile spacing effects on mesh size validity. Major parameters influencing the lateral *P-Y* curve of single-row piles were discussed from results derived from numerical models to achieve algebraic expression of the *P-Y* curve through the multivariate statistical method. Algebraic expressions of the *P-Y* curve and FEA results were validated using field measurements from an engineering test of PWFSs in Binzhou, China.

Table 1. Material parameters used in 3D FEA.

Cases	Site	Soil type	γ_{sat} (kN/m^3)	E_s (kPa)	μ_s	c (kPa)	φ (°)	f
CS1	Binzhou	Sludge	16.6	2220	0.49	4	1.4	0.02
CS2		Muddy clay	17.6	2540	0.47	9	5.7	0.08
CS3		Clay	18.2	3920	0.46	28.2	8.8	0.12
CS4		Silty clay	18.6	6330	0.44	16.6	11.9	0.16
CS5	Huanghua	Muddy clay	17.4	2340	0.496	15	0.8	0.01
CS6		Muddy-silty clay	17.8	2880	0.49	14	1.3	0.02
CS7		Silty clay	19.6	6020	0.45	30	10.6	0.14
CS8		Clay	18.1	4410	0.48	30	4.6	0.06
CS9	Haikou	Silty clay	18.7	5780	0.41	28.2	17.6	0.23
CS10		Muddy-silty clay	17.6	2790	0.45	10	11.0	0.14
CS11	Tianjin	Sludge	16.0	2060	0.499	3.2	0.1	0.00
CS12		Muddy clay	17.2	2470	0.49	9.1	1.2	0.02
CS13		Silty clay	19.3	11480	0.34	22.9	28.9	0.40
CS14		Clay	18.4	3720	0.48	21.2	4.9	0.06

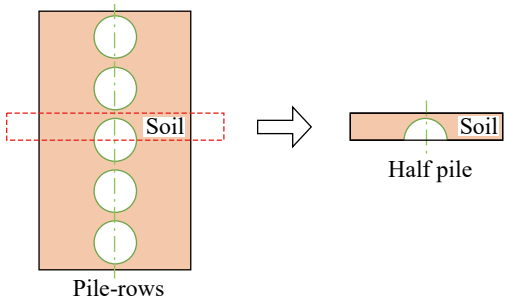

(a) Simplification process of the FE row piles model

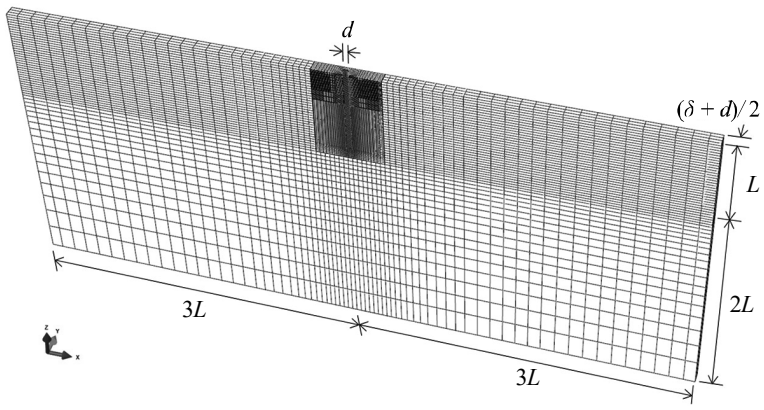

(b) Mesh of a fully 3D FE symmetry model for row piles

Fig. 2. Schematic of the finite element model.

II. FINITE ELEMENT MODEL

1. Geometry and Mesh

A series of 3D finite element models with various pile spacing (δ/d = 0.1, 0.2, 0.5, 1, 3, 8) to simulate the response of row piles subject to lateral loads in cohesive soil is presented in this section. Half of a pile and the soil between adjacent piles were selected for modeling objects in view of the symmetry

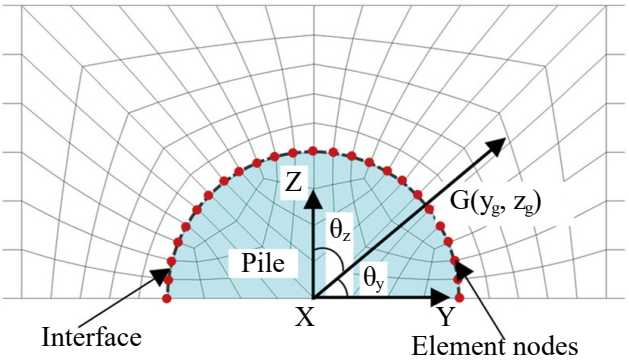

Fig. 3. Cross-section of a horizontal pile–soil system.

of row piles to save calculation costs. The typical 3D finite element mesh used to analyze laterally loaded row piles is displayed in Fig. 2. The pile length below the ground surface (L) was 20 d, and the pile top exceeded 1 d over the ground surface. The mesh boundary location was selected by extending 3 L from the center of the pile shaft in the lateral loading direction and a height of L plus 2 L below the pile toe level. These sizes were examined to ensure the P-Y curves of row piles were not affected by boundary conditions. The finite element model width on the direction perpendicular to the lateral loading was (δ + d)/2 with symmetric boundary conditions adopted on both side surfaces. Other mesh nodes at vertical boundaries were constrained to prevent out-of-plane displacement, and those at the bottom boundary were fully fixed against displacement.

The eight-node brick element was selected for both the pile and soil. The mesh tie constraint available in the numerical analysis software was adopted to connect a fine mesh (element size = 0.025–0.75 d) in the region close to the pile to a coarser mesh (element size = 0.75–2 d) on the edge to achieve time-efficient models without compromising accuracy.

2. Material Properties and Interface Conditions

The concrete pile was modeled as a linear elastic material (γ_p = 24 kN/m^3, E_p = 2.66 × 10^4 MPa, μ_p = 0.2), and the Mohr–Coulomb nonassociated flow rule (Peng et al., 2010) was selected for soil mass. The measured material properties of cohesive soil are listed in Table 1. These 14 types of soils came from different coastal areas in China and include sludge, muddy clay, clay, and silty clay soil types, with a soil cohesion of 3.2–28.2 kPa and internal friction angle of 0.1°–28.9°. Surface-to-surface contact and finite-sliding tracking were adopted to simulate the pile–soil interface. The contact property consisted of the Coulomb friction model with friction factor f (Table 1) in the tangential direction and a hard contact in the normal direction, given an allowable separation after contact.

3. Sequence of Analysis

An initial equilibrium of subsoil was conducted beforehand to generate an initial stress field matched with the self-weight of materials. Then, the pile element was activated in the model change method available in the numerical analysis software, and pile body gravity was exerted to model the pile installation process. Finally, applied loading was modeled by applying lateral displacement at pile top (e = 1 m). Under different soil conditions, the horizontal load applied on the pile top varies greatly when the lateral bearing capacity per unit of pile length reaches the ultimate value P_u, whereas the lateral displacement of pile body corresponding to P_u is a relatively constant value of approximately 0.05 d (Georgiadis, 2013). Therefore, displacement loading was used in this study to ensure the complete P-Y curve was available under different soil conditions.

4. P-Y Curve Determination

According to the relative soil–pile stiffness of $E_pI_p/E_sl_L^4$ proposed by Poulos and Hull (1989), the single pile models employed in this study have a relative soil–pile stiffness of 0.0057–0.0317, which belong to the semirigid pile ($E_pI_p/E_sl_L^4$ = 0.0025–0.208). Research results (Haiderali et al., 2015; Hong et al., 2017) have revealed that for a single pile—be it a flexible, semirigid, or rigid pile—a wedge mechanism of soil flow is always applicable near the ground surface. For small-spaced row piles, the horizontal soil flow around the pile is partially blocked, and the range of wedge mechanism is enlarged. This study mainly focused on the P-Y curve of the shallow soil area where a wedge mechanism was adopted.

To obtain and compare P-Y curves at various depths, ten reference points were selected along the pile body within 6 d below the ground surface. Slices of soil with 0.1-d thickness were cut out by considering each reference point the center. This thickness was determined by the minimum mesh size and computational accuracy. A cross section of a pile–soil system under a lateral load in the y-direction is illustrated in Fig. 3, where the soil element nodes in the pile–soil interface are marked by red dots. Soil resistance at each reference point was acquired by summing the y-component of the total contact stresses at the red dots along the pile circumference and averaging them within each soil slice with a height of Δh. Considering the finite element model symmetry, soil resistance per unit length of pile subjected to lateral loads is expressed as follows:

$$P = 2\sum\left(\sigma_{yx}^k n_x^k + \sigma_{yy}^k n_y^k + \sigma_{yz}^k n_z^k\right)A^k / \Delta h \tag{1a}$$

$$\sigma_{yi}^k = \sum_{j=1}^{4} \sigma_{yi}^{kj} / 4 \qquad (i = x, y, z) \tag{1b}$$

Given the mesh size and accuracy requirements of the model, the height range was defined as $\Delta h = 0.1d$ in this study.

Table 2. *N* values obtained from this study and other research.

	Analysis type	Roughness of interface	*N*
This study	FEA	0.001~0.4	8.4~11.0*
Matlock 1970	Empirical	——	9
Reese et al. 1975	Empirical	——	11
Wu et al. 1998	Empirical	——	10 (OCR=1) 7.7 (OCR>5)
Randolph & Houlsby 1984	Lower bound	0	9.14
		1	11.94
Martin & Randolph 2006	Upper bound	0	9.20
		1	11.94

*:*N* values in this study are derived from *P-Y* curves at a depth of $x = 6\ d$. Results of soils with large frictional angles are not included in the statistics.

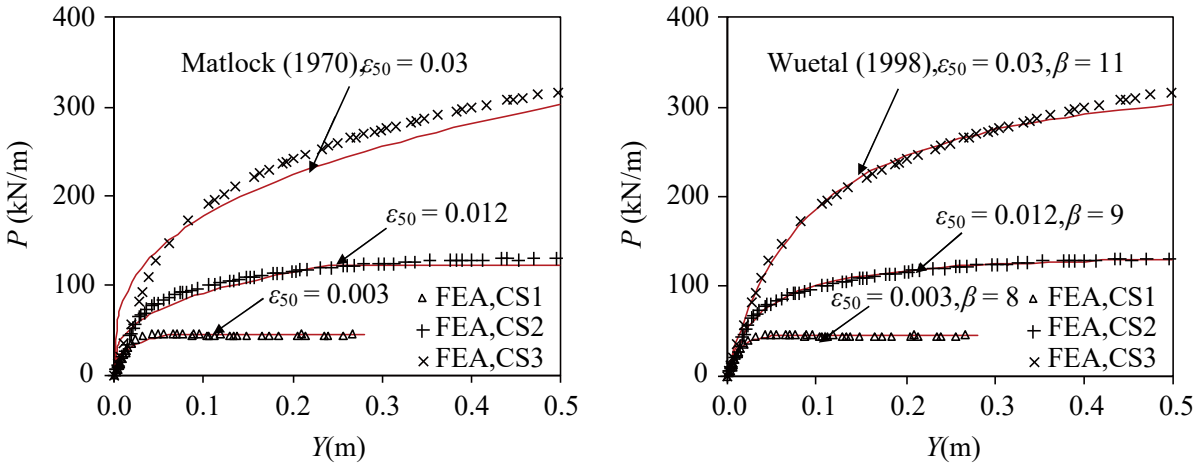

(a) Comparison with the Matlock curve (b) Comparison with the hyperbolic curve

Fig. 4. Comparison of *P-Y* curves for a single pile ($x/d = 4$).

The *P-Y* relationship curve at a designated depth is determined by relating bearing capacity *P* to corresponding lateral pile displacement *Y* at the depth.

III. RESULTS

1. P-Y Curve of a Single Pile and Validation

The efficiency factor of parallel pile groups was close to 1.0 as the pile spacing expanding to $\delta/d = 6$ (Rao et al., 1996) or $\delta/d = 8$ (Pise, 1983). The finite element model with $\delta/d = 8$ in this study, where the lateral bearing capacity of the pile structure was hardly affected by adjacent piles, was therefore treated as a single pile structure for comparison with other row pile models with various pile spacing. The *P-Y* relationship curve for a single pile in soft clay recommended in the American Petroleum Institute (2011) was proposed from field tests by Matlock (1970), where it was artificially defined that the curve tail extends horizontally as the plastic branch occurs. A hyperbolic *P-Y* curve proposed by Wu et al. (1998) from tests in medium stiff clay is predicted as follows:

$$\frac{P}{P_u} = \frac{Y/Y_{50}}{\frac{\beta}{\beta-1} + \frac{\beta-1}{\beta-2} Y/Y_{50}}. \tag{2}$$

The value of β is a constant associated with soil property, empirically used as $\beta = 8$ for soft clay, $\beta = 9$ for medium stiff clay, and $\beta = 11$ to 12 for stiff clay.

The *P-Y* curves derived from the FEA of CS1, CS2, and CS3 were compared with results obtained from empirical formulas by Matlock (1970) and Wu et al. (1998; Fig. 4). The finite element results agreed better with those by Wu et al. (1998), particularly when pile deflection was relatively small. Because $\varphi > 0$ in CS1, CS2, and CS3, the values of *P* in FEA continued to increase with the horizontal coordinate.

The ultimate lateral bearing capacity per unit length of pile

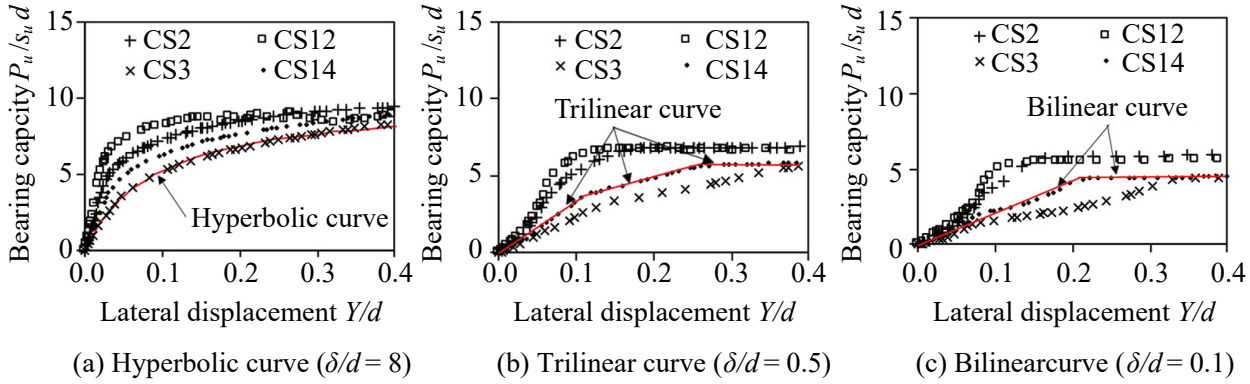

Fig. 5. Change in shapes of normalized *P-Y* curves with pile spacing (*x/d* = 4).

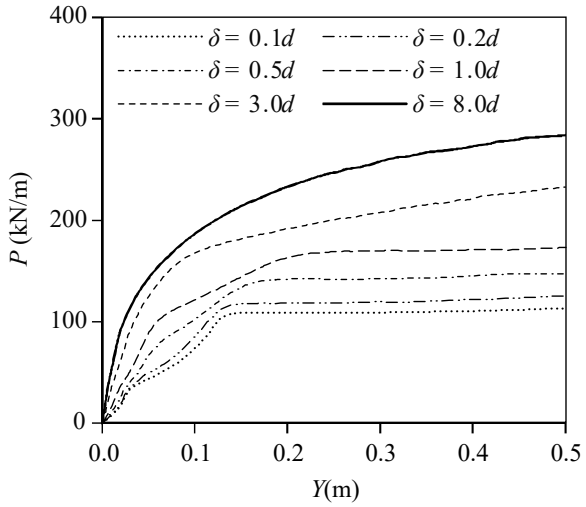

Fig. 6. Effects of pile spacing on *P-Y* curves of row piles (CS4, *x/d* = 3).

in Equation (2) mathematically equals the value of P responding to $Y = \beta Y_{50}$. Namely, the value of P_u by Wu et al. (1998) is equal to that by Matlock (1970) for soft clay (β = 8) and is larger than Matlock's results for stiff clay (β > 8). The P_u determined by Wu et al.'s method in this study was compared with other results. Generally, the ultimate lateral bearing capacity per unit length of pile in cohesive soil can be described by a dimensionless factor:

$$N = \frac{P_u}{s_u d}. \tag{3}$$

The values of N obtained from this study are summarized in Table 2 with predictions from other research. Because bearing capacity factor N is expected to vary with depth and N results from other research have concerned deep soil, the comparison in Table 2 concerns finite element results of N at a relatively deep $x = 6d$. Finite element results generally fall within the lower and upper bounds of research. Matlock (1970) assumed that the N value increases linearly from 3 at the ground surface to 9 in a deeper area. In several cases, the N values were less than 9 in Table 2, which indicated that the critical depths for those cases were larger than 6 d. For CS10 (N = 8.4), the critical depth was 8 d under the soil surface according to Matlock's method.

The *P-Y* curves of the single pile derived from FEA generally agreed with those of other research in both the curve shape and ultimate soil pressure per unit length of pile.

2. P-Y Curves of Row Piles

(1) Pile Spacing Effect

Normalized horizontal soil resistance $P_{-8d}/s_u d$ and the dimensionless horizontal displacement Y/d were adopted to eliminate the influence of soil shear strength. Normalized *P-Y* curves with various pile spacing acquired from FEA of CS2, CS3, CS12, and CS14 are compared in Fig. 5 and imply that the *P-Y* curve shape varies with pile spacing.

① The normalized *P-Y* curve of row piles with a large pile spacing of $\delta/d \geq 3$ was similar to the hyperbolic curve of a single pile (Fig. 5 [a]), which was irrelevant to the soil property.

② The normalized *P-Y* curve of row piles with a middle pile spacing of $3 > \delta/d > 0.2$ was transformed gradually from a hyperbolic curve to a bilinear curve as pile spacing decreased, where soils such as CS3 and CS14 were in a transitional state of a trilinear curve (Fig. 5 [b]).

③ The normalized *P-Y* curve of row piles with a small pile spacing of $\delta/d \leq 0.2$ was a bilinear curve with the curve tail extending horizontally (Fig. 5 [c]), which was irrelevant to the soil property.

The lateral *P-Y* curves of row piles changing with pile spacing are compared in Fig. 6 for CS2, CS3, CS4, and CS14. At a fixed depth of $x = 3$ d, both K_i and P_u in *P-Y* curves were nonlinearly reduced with the decrease in pile spacing. The inflection point of *P-Y* curves gradually became apparent, and the slope of curve tails declined as pile spacing decreased from 8 to 0.1 d. For $\delta/d \leq 0.5$, the P value nearly no longer increased with pile displacement after the *P-Y* curve inflection point, similar to the shape of the ideal plastic constitutive model.

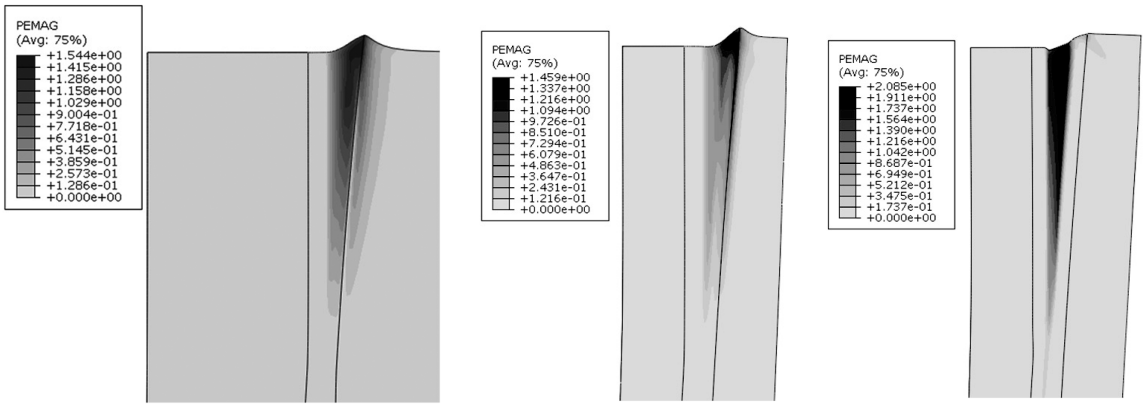

(a) $\delta/d = 8$ (b) $\delta/d = 1$ (c) $\delta/d = 0.1$

Fig. 7. Plastic strain magnitude distribution nephogram (CS3).

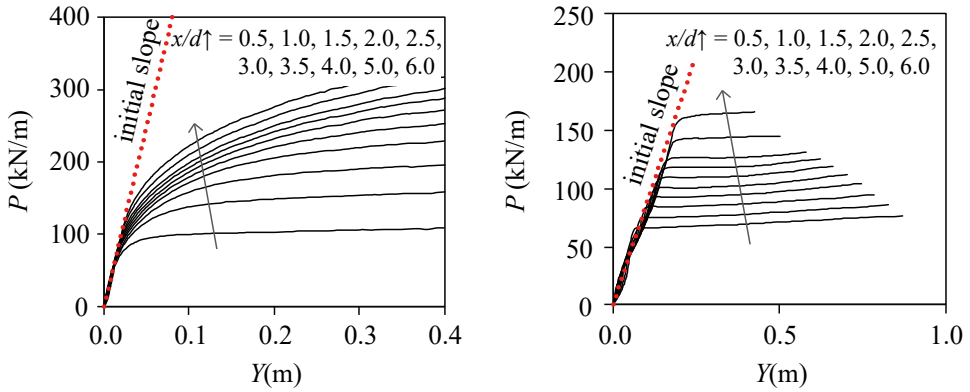

(a) CS4, $\delta/d = 8$ (b) CS4, $\delta/d = 0.1$

Fig. 8. Effects of depth on *P-Y* curves.

The plastic strain magnitude distribution (Fig. 7) acquired from finite element models can explain this result. Fig. 7 illustrates the plastic area of soil transfers from the front to the side of the pile body. As the row pile base with small spacing moved horizontally, soil resistance was mobilized only by soil mass directly in front of the pile body. The influencing area of a certain pile in the row piles was limited by adjacent piles and was difficult to expand on both sides. While the soil mass right in front of the pile body continued to deform until reaching the yield point and entering the plastic state, lateral soil resistance stopped increasing. However, the horizontal movement of the pile base with large pile spacing affected soil mass directly in front and on the side of the pile body. Thus, lateral bearing capacity increased as the influence area increased with lateral pile displacement. The soil yield was expected as the *P-Y* curve slope gradually decreased with lateral pile displacement.

(2) Depth Effect

Depth influenced the *P-Y* curve shape, and finite element results of $\delta/d = 8$ and $\delta/d = 0.1$ are compared in Fig. 8. For a single pile, the *P-Y* curve shape in the shallow soil area was significantly different from that in the deep soil area. The plastic branch of the *P-Y* curve in shallow soil was parallel to the horizontal coordinate, whereas the plastic section of the *P-Y* curve shape in the deep soil area persistently grew in *P* value. For row piles with small spacing, the depth rarely influenced the curve shape. The *P-Y* relationship remained bilinear from an area close to the ground surface to the deeper area.

Guo (2013) proposed that the initial *P-Y* curve slope for a single pile (K_{i-8d}) has no relationship with depth, and the K_{i-8d} of a long flexible pile laterally loaded on the pile top could be estimated from Equation (4) given the relative soil–pile rigidity.

$$K_{i\text{-}8d}/G = \left(6.86 + \frac{e/L}{0.1458 + 0.2834e/L}\right)\left(\frac{E_p}{G^*}\right)^{-\left[0.087 + e/L/(11.49 + 50e/L)\right]}. \quad (4)$$

FEA results indicated that the above rule remained valid as pile spacing decreased, as shown in Fig. 8. Although K_i

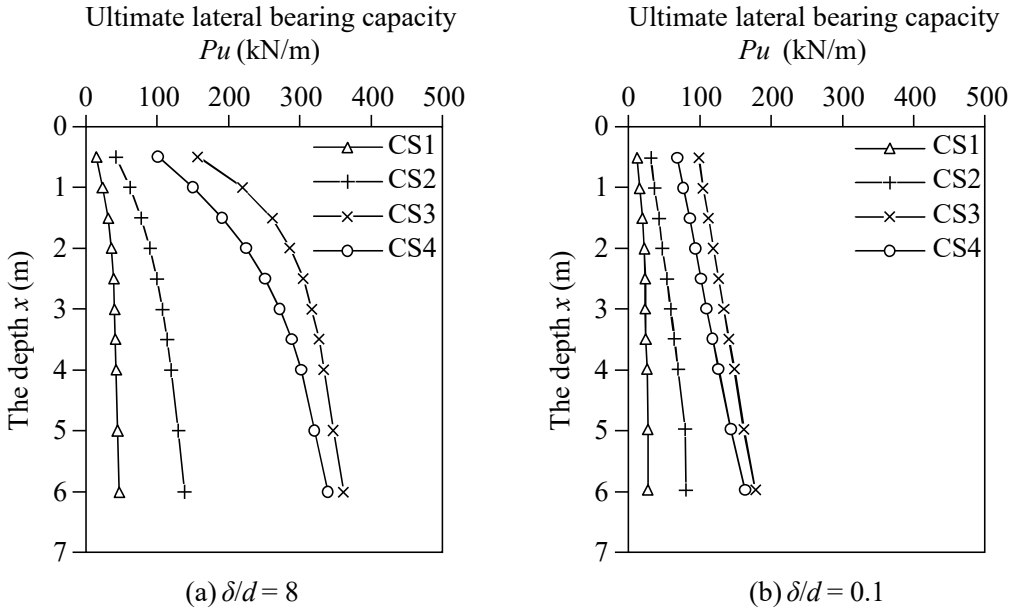

Fig. 9. Comparison of change in Pu with depth.

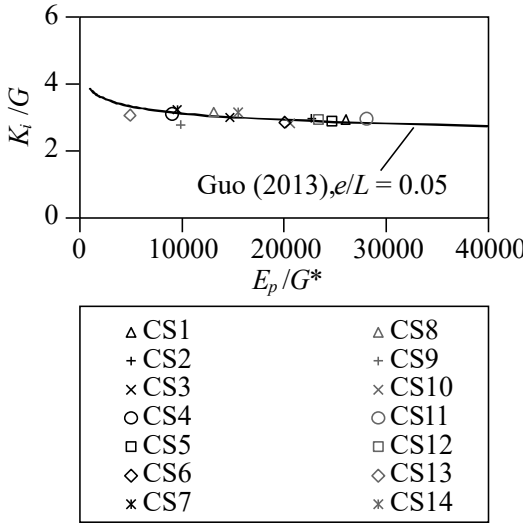

Fig. 10. Initial slope of *P-Y* curve for laterally loaded single pile.

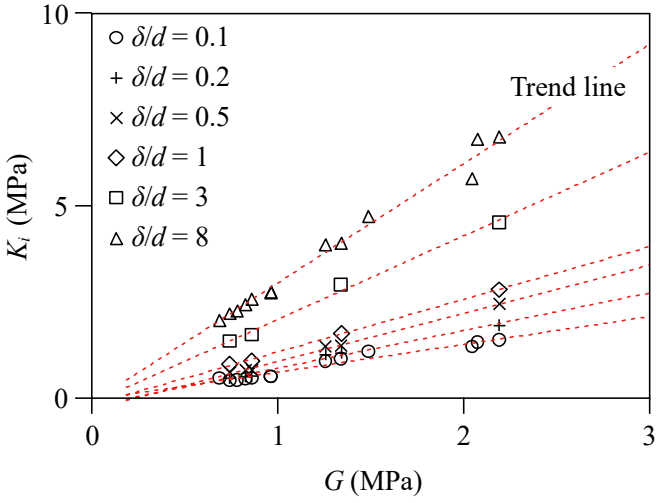

Fig. 11. Initial slope of *P-Y* curve for row piles.

decreased with decreasing pile spacing, under fixed pile spacing, *P-Y* curves at different depths had the same K_i value.

Ultimate lateral bearing capacity increased with the increase in the depth below the ground. The variation of P_u with depth (x) for a pile spacing of δ/d = 8 and δ/d = 0.1 are compared in Fig. 9. For the single pile, the P_u-x relationship had a clear inflection point. Given stratification on a single pile, Randolph and Gourvenec (2011) proposed different failure mechanisms for shallow and deep soil areas. The shallow failure mechanism involves the failure of a wedge-shaped soil area in front of the pile body, and deeper down a flow mechanism becomes critical to explain the soil flow within a hori zontal plane around the pile shaft. The P_u-x relationship is highly linear for small-spaced row piles, as displayed in Fig. 9 (b). Namely, with the decrease in pile spacing, adjacent piles restrict the soil flow around the pile shaft, and the wedge failure mechanism continues to play a key role in the deep soil area.

(3) Soil Property Effect

The initial slope of the *P-Y* curve obtained from FEA in present study was compared with that derived from Equation (4) for e/L = 0.05, as presented in Fig. 10. The ratio of initial slope to soil shear modulus (K_i/G) decreased slightly with relative soil–pile rigidity (E_p/G^*), as proposed by Guo (2013). The finite element results of K_i/G agreed well with the theo retical prediction, with minor underestimation for smaller soil–pile rigidity.

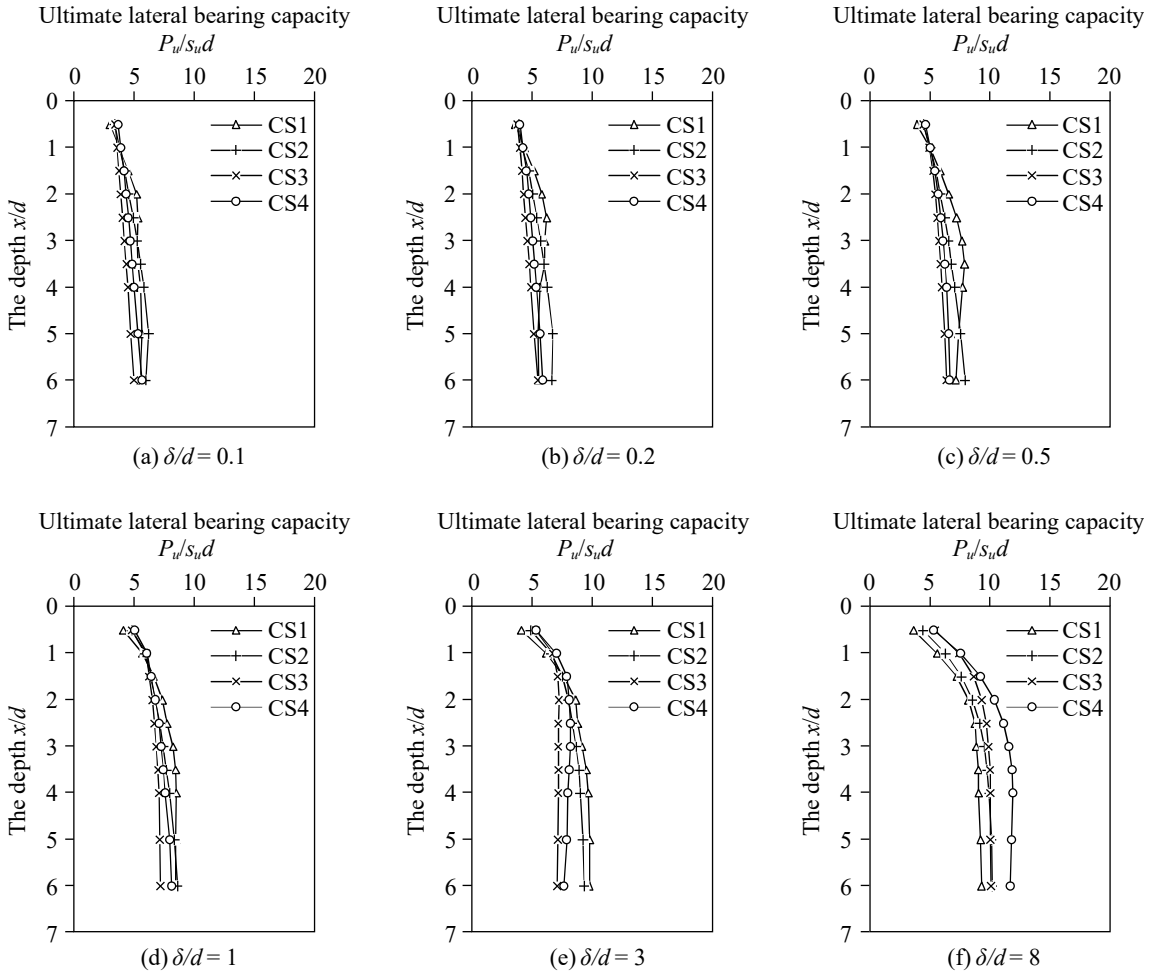

Fig. 12. Profile of normalized ultimate lateral bearing capacity.

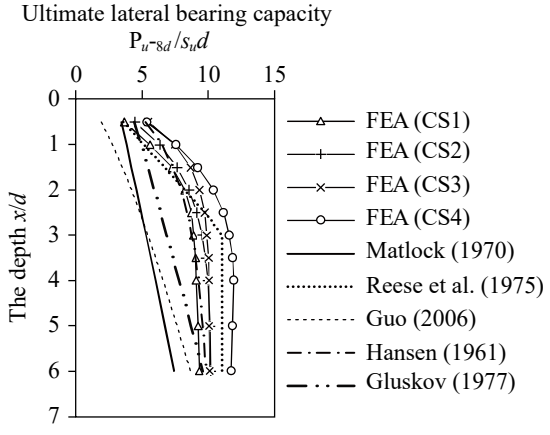

Fig. 13. Comparison of $P_{u-8d}/s_ud-x/d$ obtained from FEA and empirical expression.

The relationship between the initial slope of the *P-Y* curve (K_i) and shear modulus of soil (G) under different pile spacing are compared in Fig. 11. The finite element results revealed that K_i maintained a strong linear correlation with G for both single and row piles and the trend line slope indicated by the red dotted line in Fig. 11, which increased with pile spacing.

Research has indicated that P_u is significantly affected by the undrained shear strength of soil (s_u). Therefore, the P_u–x profile from FEA was normalized as the P_u/s_ud–x/d curve to study the soil property effects on ultimate lateral bearing capacity, as compared in Fig. 12. The normalized curves of P_u/s_ud–x/d were alike with different soils. Namely, the effects of soil property on the bearing capacity of the pile could be eliminated somewhat through normalization. Then, the P_u/s_ud value was mainly affected by pile spacing and depth.

The P_{u-8d}/s_ud–x/d curves obtained from FEA were compared with other empirical expressions, as displayed in Fig. 13. Studies have generally posited that $P_{u-8d}/s_ud = 2$ to 4 at the soil surface ($x/d = 0$). FEA results revealed that $P_{u-8d}/s_ud = 3.6$ to 5.4 at $x/d = 0.5$. Due to soil mass discreteness, current empirical formulas differ considerably from each other. Until now, no fully satisfactory unified expression has ever been identified. The finite element results of the P_{u-8d}/s_ud–x/d relationship generally agreed with current empirical expressions, with exceptional overprediction for CS4 due to its larger internal friction angle of soil.

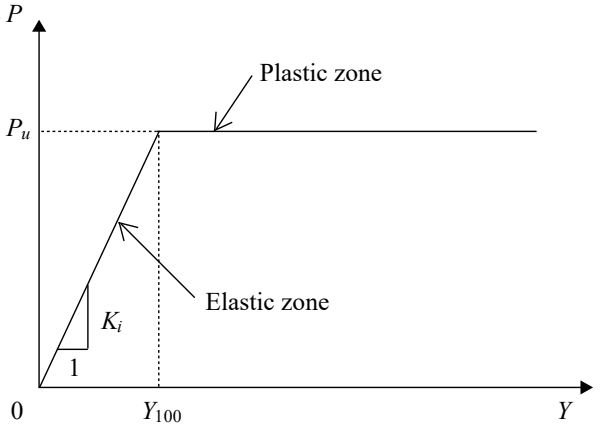

Fig. 14. *P-Y* curve of row piles with small pile spacing.

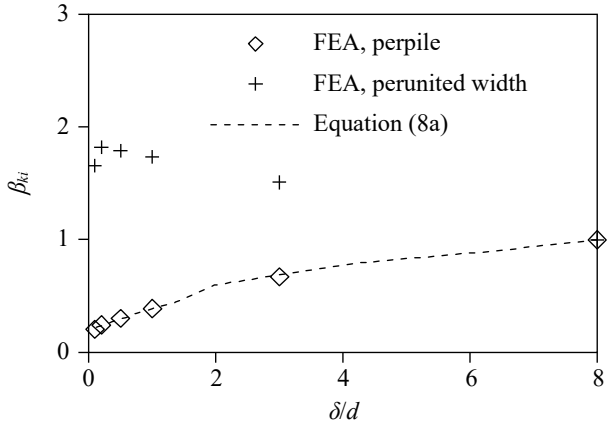

Fig. 15. Fitting results of reduction coefficient β_{Ki}.

3. P-Y Curve Expression of Small-Spaced Row Piles

(1) P-Y Curve Bilinear Model

The pile spacing of PWFSs was approximately 0.1–0.5 *d* to satisfy soil-retaining and bearing capacity requirements and was smaller than that of normal pile structures. Therefore, this study focused on bilinear *P-Y* curve expression composed of a linear elastic segment and an ideal plastic segment that was suitable for predicting the behavior of laterally loaded row piles with small pile spacing. As illustrated in Fig. 14, bilinear *P-Y* curve expression could be determined by two parameters: ultimate lateral bearing capacity (P_u) and the initial slope of the *P-Y* curve (K_i).

$$P=\min\left\{P_u, K_iY\right\}. \tag{5}$$

These two parameters could be derived from other parameters such as pile spacing, buried depth, soil property, and the bending stiffness of the pile.

(2) Fitting Results of P_u for Row Piles

This parameter study indicated that the ultimate lateral bearing capacity per unit length of pile (P_u) was affected by pile spacing, depth, and soil property. The expression of the ultimate lateral bearing capacity of row piles ($\delta/d < 3$ *d*) can be fitted through stepwise multiple regression analysis on data derived from the FEA of all 14 groups of soils. During stepwise regression, factors with insignificant influence should be eliminated, such as the unit weight of soil and pile stiffness. The dependent variable and independent variables are normalized as P_u/s_ud, δ/d, x/d, and s_u/E_s to eliminate the dimension effect between indicators, while the internal friction angle adopts the radian system ($\overline{\varphi}$). Therefore, the ultimate lateral bearing capacity of row piles can be estimated approximately
from Equation (6) as follows:

$$N=3.65+1.27\frac{\delta}{d}+0.54\frac{x}{d} +4.12\overline{\varphi}-0.19\times10^3\frac{s_u}{E_s}\quad\left(0\le\delta/d\le3\right), \tag{6a}$$

$$P_u=Ns_ud \tag{6b}$$

(3) Fitting Results of K_i for Row Piles

Based on the parameter study, the initial slope of the *P-Y* curve (K_i) was mainly affected by pile spacing and relative soil–pile rigidity. A comparison of FEA results and Equation (4), which was proposed by Guo (2013), in Fig. 10 indicates that Guo's method was feasible for predicting the initial slope of the *P-Y* curve for the single pile. The K_i–G relationship under different pile spacing is compared in Fig. 11, from which the slope of each trend line (K_i/G) was extracted. A reduction coefficient β_{Ki} was used to measure the influence of pile spacing on slope, which was denoted as $\beta_{Ki} = (K_i/G)/(K_{i-8d}/G) = K_i/K_{i-8d}$. A quadratic polynomial was adopted to estimate the variation of β_{Ki} with δ/d under constraint conditions shown as the following:

$$\begin{cases}\beta_{K_i}|_{\delta/d=8}=1\\ \beta'_{K_i}|_{\delta/d=8}=0\end{cases} \tag{7}$$

The fitting results are illustrated as follows:

$$\beta_{K_i}=-0.0126\left(\delta/d\right)^2+0.2016\left(\delta/d\right) +0.1936\quad\left(0\le\delta/d\le8\right), \tag{8a}$$

$$K_i=\beta_{K_i}K_{i\text{-}8d}, \tag{8b}$$

compared with FEA results in Fig. 15. Therefore, the initial slope of the *P-Y* curve for row piles with small spacing could be obtained from Equations (4) and (8).

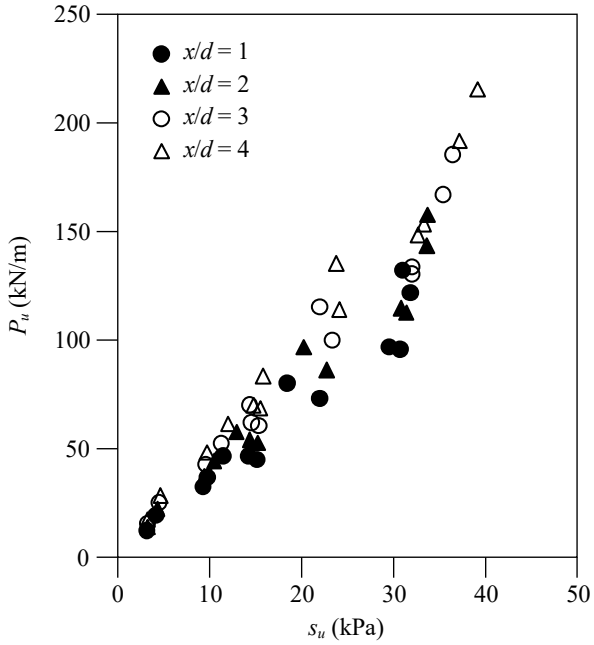

Fig. 16. Change in P_u with s_u.

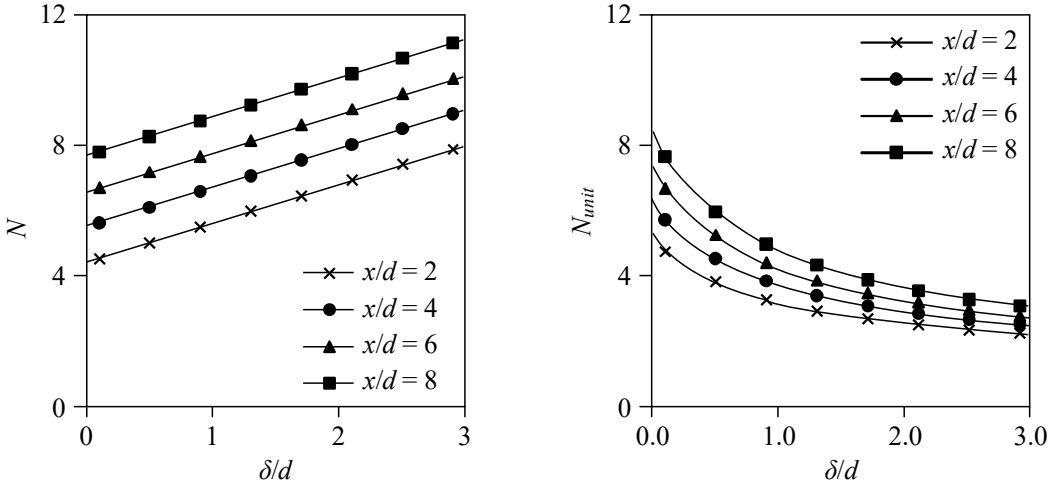

(a) Bearing capacity per pile of N (b) Bearing capacity per unit width of N_{unit}

Fig. 17. Comparison of ultimate bearing capacity for various depths and pile spacing.

(4) Parameter Study on the Bilinear P-Y Curve

The effect of the undrained shear strength of soil (s_u) on ultimate bearing capacity per unit length of row piles (P_u) was studied. When $\delta/d = 0.1$, the scatter diagram P_u−s_u illustrated in Fig. 16 by using Equation (6) with a depth of x/d ranged from 1 to 4 in homogeneous soil. The soil properties were the same as those used in the FEA (Table 1). The P_u value grew at a high rate at deep locations because the s_u value linearly increased with depth.

The effect of pile spacing (δ/d) and depth (x/d) on ultimate bearing capacity per unit length of row piles was investigated. The relationships of N−δ/d at various depths are compared in Fig. 17(a) based on results from Equation (6). The homogeneous soil of CS2 was adopted with a pile spacing of δ/d ranging from 0 to 3 and a depth of x/d ranging from 2 to 8. The computational results indicated that the dimensionless ultimate bearing capacity of N increased uniformly with pile spacing and depth. A dimensionless factor of bearing capacity per united width defined as $N_{unit} = P_u/s_u(d + \delta) = N/(1 + \delta/d)$ was employed to estimate the bearing capacity of row piles with different pile spacing. The comparison results of Fig. 17(b) indicated that N_{unit} nonlinearly decreased with an increasing in δ/d. N_{unit} decreased rapidly with the change of δ/d

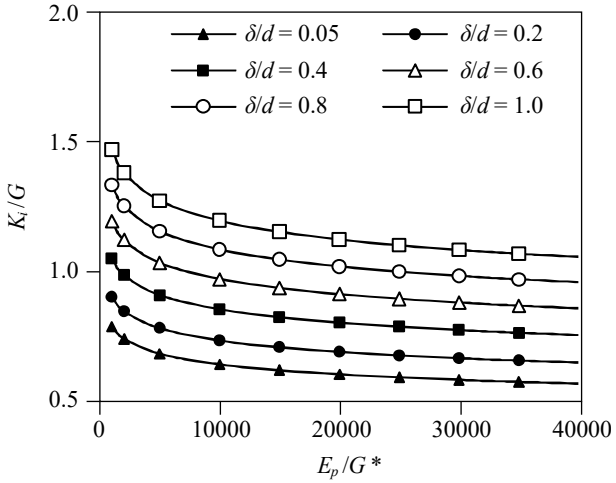

Fig. 18. Change in K_i/G with E_p/G^*.

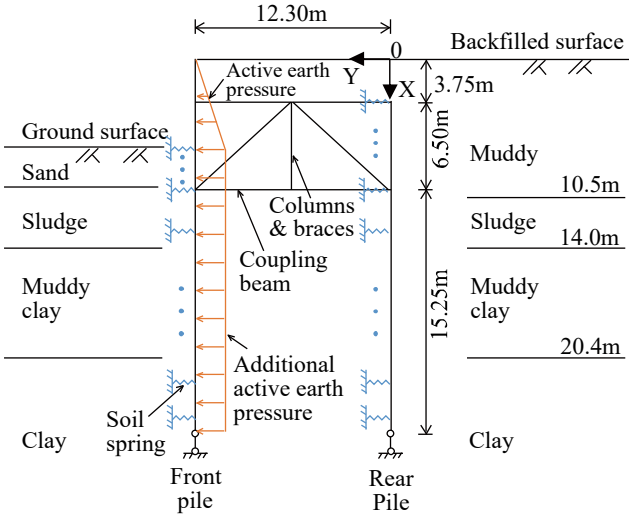

Fig. 19. Schematic of the plane finite element model for an engineering test.

from 0 to 1, then slowed down as δ/d continued to increase. Compared with a single pile or pile groups with large pile spacing, small-spaced row piles benefitted lateral bearing capacity. A small pile interval always signifies more costs; thus, balancing the contradiction between bearing capacity and cost is necessary.

The effect of the relative soil–pile rigidity (E_p/G^*) and pile spacing (δ/d) on the initial slope of *P-Y* curves is discussed. The K_i/G–E_p/G^* relationships at various pile spacings are compared in Fig. 18 based on results from Equations (4) and (8). The E_p/G^* ratio changed from $1.0e^3$ to $4.5e^4$ with a pile spacing of δ/d ranging from 0.05 to 1. The change regulation of K_i/G ratio decreasing with increasing relatively soil–pile rigidity remained valid for row piles with a small pile spacing K_i/G ratio. The K_i/G ratio reduced with the decrease in pile spacing; thus, the K_i/G value for row piles with small pile spacing was much less than that for single piles (Fig. 10).

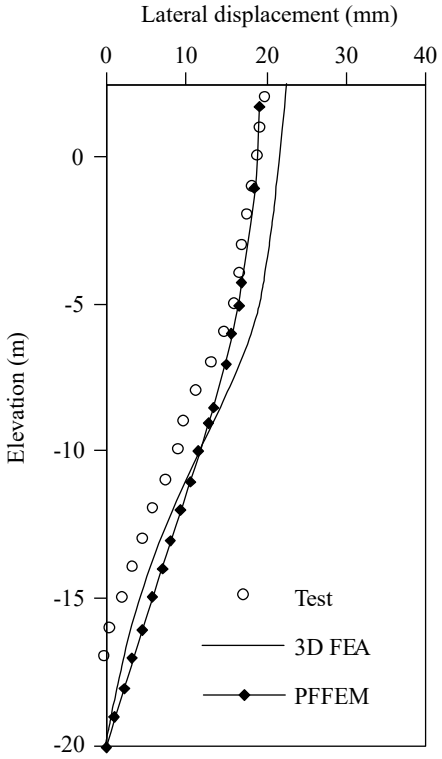

Fig. 20. Comparison of lateral displacement curves.

4. Comparison with Engineering Test

The proposed *P-Y* curve model could be combined through the subgrade reaction method to predict the behavior of row piles with small spacing subject to lateral loads. One example of the engineering test for PWFS in Binzhou, China, was considered to demonstrate the effect of the fitted *P-Y* curve expression.

(1) Plane Finite Element Model

The PWFS engineering test adopted for a cofferdam in Binzhou employed a pile base of PHC pipe piles, with a tiny pile spacing of 0.1 *d* (*d* = 1 m). The marine deposits in the engineering site consisted of sludge, muddy clay, and clay, with an undrained shear strength of approximately 7–37 kPa. Backfilling behind the PWFS cofferdam was muddy clay excavated from a nearby waterway, and sandbags were pressed on the ground surface in front of the PWFS to maintain its stability because the backfilling was unconsolidated. The PWFS can be simplified as a plane structure to build the finite element model given its structural symmetry. The plane finite element model is illustrated in Fig. 19, where the structure is modeled by the beam element and soil–pile interaction is modeled by a series of soil springs. Combined with the material parameters listed in Table 3, the plane finite element model could be solved through self-made FORTRAN program Plane Frame Finite Element Method (PFFEM) by using stiffness coefficients of soil springs deduced from the proposed *P-Y* curve expression for row piles with small spacing.

Table 3. Material parameters used in the plane finite element model.

Type		Element	EA (kN)	EI (kN·m^2)	s_u (kPa)	φ (°)	E_s (kN/m^2)
Structure	Pile	Beam	1.72×10^7	1.08×10^6	——	——	——
	Coupling beam		4.93×10^6	9.26×10^5	——	——	——
	Side-column		2.44×10^7	3.99×10^6	——	——	——
	Mid-column		1.97×10^6	5.92×10^4	——	——	——
	Brace		1.97×10^6	5.92×10^4	——	——	——
Soil	Muddy	Soil spring	——	——	3.0	0.1	2000
	Sludge		——	——	7.2	1.4	2220
	Muddy clay		——	——	12.4	5.7	2540
	Clay		——	——	36.7	8.8	3920
	Sand		——	——	——	28	2×10^4

Note：Items listed are converted into value per unit width.

(2) Comparison of Lateral Pile Displacement

The lateral displacement curve of the front pile derived from PFFEM was compared with observed data from the engineering test, as shown in Fig. 20, and contrasted with results from the 3D finite element method of the PWFS analyzed using numerical analysis software. The lateral displacement curves along the pile shaft in numerical analysis, both 3D FEA and PFFEM, generally agreed well with observations from the engineering test. All result curves reflected the similar characteristic that changes in rotation angle and the horizontal displacement of pile body were unclear in a range of −5 to 2.5 m, which indicated the effective restraint of the frame structure to the pile body. The proposed *P-Y* curve was indicated to have good performance in predicting the behavior of the PWFSs observed from an engineering test.

IV. CONCLUSIONS

This study mainly numerically investigated the *P-Y* curve of laterally loaded single-row piles in marine clay, particularly for row piles with small spacing ($\delta/d < 3$). In this study, the nonlinear 3D finite element model for small-spaced row piles was presented and discussed by considering pile–soil interaction continuity on the basis of geological survey data of offshore deposits obtained from Chinese coastal areas. The simulation method was examined, and the analysis results were verified by comparing the *P-Y* curve from the single pile finite element model ($\delta/d = 8$) with current empirical expressions. Then, influences of pile spacing, buried depth and soil property on the *P-Y* curve were studied through finite element models of row piles in homogeneous soil with pile spacing ranging from 8 to 0.1 *d*. In addition, the *P-Y* curve type suitable for row pile structures with small spacing was suggested, with detailed expressions for ultimate bearing capacity and the initial slope of the *P-Y* curve. From the study findings, the following conclusions could be drawn:

1. Considering the small pile spacing effect, the *P-Y* expression proposed by a bilinear curve was an appropriate and realistic representation of the pile–soil interactions of single-row piles with small spacing subject to lateral load in marine soil. With the subgrade reaction method, the proposed *P-Y* function could provide the lateral displacement of row pile structures with small spacing in good agreement with the field test result.
2. Significantly different from the hyperbolic *P-Y* curve of the single pile, the *P-Y* curve of row piles with small spacing was similar to the elastic–perfectly plastic curve (i.e., a bilinear curve). Therefore, the *P-Y* curve of row piles with small spacing could be determined directly by two parameters: ultimate lateral bearing capacity (P_u) and the initial slope of the *P-Y* curve (K_i).
3. Parametric studies have indicated that both P_u and K_i increase nonlinearly with decreasing pile spacing. For both single and row piles, K_i was hardly influenced by buried depth. Regarding row piles with small spacing, adjacent piles restricted soil flow around the pile shaft and resulted in the wedge mechanism, which continues to play a key role in soil depth. Thus, the P_u of row piles increased approximately with constant speed as depth increased. For row piles in marine soil with small pile spacing, the K_i was positively correlated with the shear modulus of soil, and P_u was positively correlated with the undrained shear strength of soil.

ACKNOWLEDGEMENTS

This research was funded by the Tianjin Key R & D Plan (18YFZCSF00490) and the Tianjin marine development with science and technology project (Nos.KJXH2014-11). This research was supported by Tianjin Port Engineering Co. Ltd., which was responsible for engineering application construction. This manuscript was edited by Wallace Academic Editing.

NOMENCLATURE

A^k the area of soil element k;
c cohesion of soil;
d diameter of pile;
e eccentricity of the applied load above ground surface;
E_p equivalent Young's modulus of pile, $E_p = (EI)_p \big/ (\pi d^4/64)$;
E_s Young's modulus of soil;
f friction factor on the pile-soil interface;
G shear modulus of soil;
G^* equivalent shear modulus of soil, $G^* = (1+0.75\nu)G$;
I_p moment of inertia of the pile section;
K_i initial slope of P-Y curve;
$K_{i\text{-}8d}$ initial slope of P-Y curve for single pile;
L Embedded depth of pile in the FE model;
N dimensionless factor of bearing capacity per pile, $N=P_u/s_u d$;
N_{unit} dimensionless factor of bearing capacity per united width, $N_{unit}=P_u/s_u(d+\delta)$;
n_x^k, n_y^k, n_z^k the component of unit normal along the x-, y-, z-direction at nodes of the soil element k;
P lateral bearing capacity per unit length of pile in a row;
P_u ultimate lateral bearing capacity per unit length of pile in a row;
$P_{u\text{-}8d}$ ultimate lateral bearing capacity per unit length of single pile;
s_u undrained shear strength of soil;
x depth below ground surface;
Y lateral pile displacement;
Y_{50} lateral pile displacement as P=0.5P_u in the P-Y curve;
Y_{100} lateral pile displacement as $P=P_u$ in the P-Y curve;
β the coefficient from triaxial tests;
β_{Ki} reduction coefficient, $\beta_{Ki}=K_i/K_{i\text{-}8d}$;
γ_p unit weight of pile;
γ_{sat} saturated unit weight of soil;
δ pile spacing;
μ_p Passion radio of pile;
μ_s Passion radio of soil;
$\sigma_{yx}^k, \sigma_{yy}^k, \sigma_{yz}^k$ the component of average stress of the soil element k;
$\sigma_{yx}^{kj}, \sigma_{yy}^{kj}, \sigma_{yz}^{kj}$ the component of stresses at four nodes of the soil element k, j=1, 2, 3, 4;
φ internal friction angle, degree system;
$\bar{\varphi}$ internal friction angle, radian system.

REFERENCES

Aminfar, A., A. Mojtahedi, H. Ahmadi and M. H. Aminfar (2015). Behavior of pile group with elevated cap subjected to cyclic lateral loads. China Ocean Eng. 29(4), 565-578.

API (American Petroleum Institute) (2011). Recommended practice 2-GEO geotechnical and foundation design considerations, 1st edn. Washington, DC, USA: American Petroleum Institute.

Chandrasekaran, S. S., A. Boominathan and G. R. Dodagoudar (2010). Group interaction effects on laterally loaded piles in clay. J. Geotech. Geoenviron. Eng. 136(4), 573-582.

Conte, E., A. Troncone and M. Vena (2013). Nonlinear three-dimensional analysis of reinforced concrete piles subjected to horizontal loading. Comput. Geotech. 49, 123-133.

Fayyazi, M. S., M. Taiebat and W. D. L. Finn (2014). Group reduction factors for analysis of laterally loaded pile groups. Can. Geotech. J., 51(7), 758-769.

Georgiadis, K., S. W. Sloan and A. V. Lyamin (2013). Ultimate lateral pressure of two side-by-side piles in clay. Géotechnique 63(9), 733-745.

Gluskov, G. N. (1977). Design of installations embedded in soil, Moscow: Stroiizdat.

Guo, W. D. (2006). On limiting force profile, slip depth and response of lateral piles. Comput. Geotech., 33(1):47-67.

Guo, W. D. (2013). Simple model for nonlinear response of 52 laterally loaded piles. J. Geotech. Geoenviron. 139(2), 234-252.

Hansen, J. B. (1961). The ultimate resistance of rigid piles against transversal forces, Bullentin 12, The Danish Geotechnical Institute, Copenhagen, Denmark, 5-9.

Haiderali, A. E., B. H. Lau, S. K. Haigh and S. P. G. Madabhushi (2015). Lateral response of monopiles using centrifuge testing and finite element analysis. Proceedings of the 8th International Conference on Physical Modelling in Geotechnics, Perth, Australia, January, 14-17.

Hong, Y., B. He, L. Z. Wang, Z. Wang, C. W. W. Ng and D. Mašín (2017). Cyclic lateral response and failure mechanisms of semi-rigid pile in soft clay: centrifuge tests and numerical modelling. Can. Geotech. J. 54(6), 806-824.

Jeong, S., Y. Kim and J. Kim (2011). Influence on lateral rigidity of offshore piles using proposed p-y curves. Ocean Eng. 38(2), 397-408.

Khodair, Y. and A. Abdel-Mohti (2014). Numerical analysis of pile–soil interaction under axial and lateral loads. International Journal of Concrete Structures & Materials 8(3), 239-249.

Kim, Y. and S. Jeong (2011). Analysis of soil resistance on laterally loaded piles based on 3d soil–pile interaction. Comput. Geotech. 38(2), 248-257.

Kondner, R. L. (1963). Hyperbolic stress-strain response: Cohesive soils. J. Soil Mech. and Found. Div. 89(1), 115-143.

Li, W., P. L. Zhang, S. A. Bie, Z. J. Li, X. Li, X. Liu and L. F. Mi (2013). Pile wall frame structure. Chinese Patent, CN 103276691A.

Martin, C. M. and M. F. Randolph (2006). Upper-bound analysis of lateral pile capacity in cohesive soil. Géotechnique 56(2), 141-146.

Matlock, H. (1970). Correlations for design of laterally loaded piles in soft clay. Proc., 2nd Offshore Technology Conf., Dallas, 577-594.

McClelland, B. and J. A. Focht (1958). Soil modulus for laterally loaded piles. Trans. ASCE, 123, 1049-1086.

Murphy, G., D. Igoe, P. Doherty and K. Gavin (2018). 3D FEM approach for laterally loaded monopile design. Comput. Geotech. 100, 76-83.

Peng, J. R., M. Rouainia and B. G. Clarke (2010). Finite element analysis of laterally loaded fin piles. Comput. Struct. 88(21), 1239-1247.

Pise, P. J. (1983). Lateral load-deflection behaviour of pile groups. Indian

Geotech. J. 13, 37-51.

Poulos, Harry and T. S. Hull (1989). Role of analytical geomechanics in foundation engineering. Foundation Engineering @ Current Principles and Practices. ASCE: 1578-1606.

Randolph, M. F. and S. Gourvenec (2011). Offshore Geotechnical Engineering. Florida, USA: CRC Press, 208-230.

Randolph, M. F. and G. T. Houlsby (1984). The limiting pressure on a circular pile loaded laterally in cohesive soil. Géotechnique, 34(3), 457-457.

Rani, S. and A. Prashant (2015). Estimation of the linear spring constant for a laterally loaded monopile embedded in nonlinear soil. Int. J. Geomech., 15(6), 04014090.

Rao, S. N., V. G. S. T. Ramakrishna and G. B. Raju (1996). Behavior of pile-supported dolphins in marine clay under lateral loading. J. Geotech. Engrg. 122(8), 607-612.

Reese, L. C., W. P. Cox and F. D. Koop (1975). Field testing and analysis of laterally loaded piles in stiff clay. Proc., 7th Annual Offshore Technology Conf., 671-690.

Salgado, R., F. S. Tehrani and M. Prezzi (2014). Analysis of laterally loaded pile groups in multilayered elastic soil. Comput. Geotech. 62, 136-153.

Su, D., J. J. Huang and R. W. M. Yan (2017). Parametric investigation on the responses of laterally loaded piles in overconsolidated clay using non-dimensional solutions addressing nonlinear soil-pile interaction. Computers and Geotechnics, 96, 203-214.

Sullivan, W. R., L. C. Reese and C. W. Fenske (1980). Unified method for analysis of laterally loaded piles in clay. Numerical methods in offshore piling. Proc. of a conference organized by the Institution of Civil, London, England, 135-146.

Wang, H. C. and D. Q. Wu (1991). A new united method of p-y curves of laterally statically loaded piles in clay. J. Hohai Univ. (Natural sciences), 19(1), 9-17.

Wu, D. Q., B. Broms and V. Choa (1998). Design of laterally loaded piles in cohesive soils using p-y curves. Soils Found. 38(2), 17-26.

Xue, R. Z., S. A. Bie, L. L. Guo and P. L. Zhang (2019). Stability analysis for cofferdams of pile wall frame structures. KSCE Journal of Civil Engineering, 23(9), 4010-4021.

Zhang, W. (2018). Ultimate lateral capacity of rigid pile in c–φ soil. China Ocean Eng., 32(1), 41-50.

Zhang, Y., K. H. Andersen and G. Tedesco (2016). Ultimate bearing capacity of laterally loaded piles in clay – some practical considerations. Marine Structures, 50, 260-275.

Zhu, B., Y. X. Sun, R. P. Chen, W. D. Guo and Y. Y. Yang (2015). Experimental and analytical models of laterally loaded rigid monopiles with hardening p–y curves. J. Waterw. Port. C.-ASCE. 04015007.